Journal of Alloys and Compounds 682 (2016) 338–344

Contents lists available at ScienceDirect

Journal of Alloys and Compounds

journal homepage: http://www.elsevier.com/locate/jalcom

Thorough investigations of the structural and electronic properties of $Al_xIn_{1-x}N$ ternary compound via ab initio computations

Yee Hui Robin Chang [a, b, *], Tiem Leong Yoon [b], Thong Leng Lim [c], Maksim Rakitin [d]

[a] Faculty of Applied Sciences, UiTM Sarawak, 94300, Samarahan, Sarawak, Malaysia
[b] Universiti Sains Malaysia, 11800 USM, Penang, Malaysia
[c] Faculty of Engineering and Technology, Multimedia University, Jalan Ayer Keroh Lama, 75450, Melaka, Malaysia
[d] Department of Geosciences, Stony Brook University, Stony Brook, NY, 11794-2100, USA

ARTICLE INFO

Article history:
Received 28 February 2016
Received in revised form
25 April 2016
Accepted 26 April 2016
Available online 27 April 2016

Keywords:
$Al_xIn_{1-x}N$
Variable-composition mode
Ab initio calculations
Electronic properties
Convex hull

ABSTRACT

Numerous experimental studies have shown that the formulation of a quality $Al_xIn_{1-x}N$ crystal is undeniably challenging, due to mismatch of certain physical properties between its parent blocks. Prior knowledge regarding proper mixture of aluminium and indium could be helpful in the blending of this crystal. Here, by applying ab initio crossbreed evolutionary computations, extensive search for the thermodynamically and practically stable composites of AlN–InN was performed. Set at atmospheric pressure, the comprehensive calculations brought forth a thermodynamically stable structure $Al_4In_2N_6$ ($Cmc2_1$) along with five metastable compounds in $AlIn_7N_8$ ($P3m1$), Al_5InN_6 ($P31m$), $Al_2In_4N_6$ (Cc/Aa), $Al_3In_3N_6$ (Cm/Am) and $Al_6In_2N_8$ ($P2_1$). Electronic structure calculations within Density Functional Theory and Bader charge analysis are also discussed. All structures are revealed to be mixed bonding direct semiconductor with GW corrected gap in the range of 0.5–6.0 eV.

1. Introduction

Generally, $Al_xIn_{1-x}N$ can be regarded as a mixed compound of aluminium nitride and indium nitride with properties characterized by proportion of aluminium to indium. Together with GaN, these two parent blocks (AlN and InN) are exemplifications of III–V nitride binary alloys that have drawn enormous researching interests over the past two decades, largely due to their stand-out properties such as unique band gap, high electron mobility [1], good thermal stability [2] and low sensitivity towards ionizing radiations. In the production of optoelectronic devices, a particular energy band gap is often required. Through the use of ternary, tuning of the magnitude of forbidden gaps (direct or indirect) is made possible. By and large, direct band gap ternary like $Al_xGa_{1-x}As$, $Al_xGa_{1-x}N$ and $In_xGa_{1-x}N$ are extensively studied. Emerging interest in $Al_xIn_{1-x}P$ [3], an indirect band gap material, has also been noted. However, the same enthusiasm cannot be said for $Al_xIn_{1-x}N$. The lack of exploration for this ternary compound is often attributed to the dissimilarities in covalent bond and thermal stability between AlN and InN, sequentially causing compositional inhomogeneity along with phase separation during alloy formation [4–6]. Growing high quality single crystals of these materials is in no doubt an uphill undertaking.

Despite the difficulties, interest on $Al_xIn_{1-x}N$ related studies continue to be revived sporadically [7–9]. This material remains an enticing prospect, owing to its wide coverage of electromagnetic spectrum ranging from deep ultraviolet to near infrared region. In sight of the aforementioned constraints, the need to search for possible stable and metastable crystal structures within Al–In–N system by means of theoretical forecast has become vastly momentous. By identifying an array of probable structures hypothetically, each with reliable and promising composition breakdown, the characterization and synthesis of $Al_xIn_{1-x}N$ might become more achievable. With reference to the predicted Al/In ratio, one can eliminate the possibility of having a compound grown from unreasonable initial condition. Thus far, there have been quite a number of theoretical investigations on lattice parameters and band gap energies of $Al_xIn_{1-x}N$. Most of these calculations were performed by assuming that the relaxed lattice parameters of $Al_xIn_{1-x}N$ alloys, in either wurtzite or zincblende form, are expressible as a linear combination of the lattice constants of their respective binaries [10–12].

* Corresponding author. Faculty of Applied Sciences, UiTM Sarawak, 94300, Samarahan, Sarawak, Malaysia.
E-mail address: robincyh@sarawak.uitm.edu.my (Y.H. Robin Chang).

http://dx.doi.org/10.1016/j.jallcom.2016.04.281
0925-8388/

In our case, first principle evolutionary techniques have been performed on Al–In–N system in order to obtain its stable structure at atmospheric pressure via USPEX [13–15]. Apart from chemical composition, no other initial guesses or system-specific knowledge were required. Electronic attribute of the stable composition are then attained via plane-wave method as realized in the Vienna ab initio simulation package [16,17]. Outcome of electronic structure can be used to deduce the nature of Al–In–N chemical bonds, which is needed for in depth understanding of local structure and ionic conductivity.

2. Computational methods

In order to determine all plausible stable structures in the Al–In–N system, variable-composition search was performed using USPEX code [18,19], interfaced with first principle relaxations through VASP. Calculations were fixed to tolerate up to 60 generations. Maximum number of atoms per unit cell reached was 24. 80 random structures were produced randomly from space groups with symmetry numbers of 2–230, within the first generation, while successive generations stored 40 structures apiece. All subsequent structures were produced by applying heredity (40%), random (20%), soft mutation (10%), lattice mutation (10%) and transmutation (20%) variation operators. At first, premature structures will be usually very far from local minima and their internal ions are closely packed. To avoid having under optimized structures, five relaxation stages were executed on every structure. One single job corresponds to a relaxation step. Step one was implemented with very crude computational conditions and low precision settings. Normal precision and finer computational quality were adopted in step two. Both step one and step two relaxed the cell shape and ions at constant volume. The purpose of halting the cell volume was to avert large forces on ions from causing sudden cell expansion. In the next two steps, convergence criteria were tightened and cell volume was allowed to change. Relaxation finished off with a single point energy calculation converged to within 1 meV in the final step, with both cell shape and volume being kept constant. Brillouin zone for the five relaxation stages was sampled by k-point meshes of space resolution 0.15, 0.13, 0.11, 0.09 and 0.07 $2\pi Å^{-1}$.

During structure optimization, cut-off energy for plane wave basis set was increased gradually from default value (largest ENMAX in POTCAR files) to 520 eV. Partial occupancies for each wave function in all relaxation steps were set using Methfessel-Paxton scheme. Acquired stable and metastable compounds were then reoptimized using a fully automatic Monkhorst-Pack scheme with $4 \times 4 \times 4$ k-point grid in a static self-consistent run, thus ensuring the generation of high quality charge density before moving on to electronic structure computations. Practically stable or metastable structures were defined as those with formation enthalpies less than 0.05 eV/block. Generalized gradient approximation (GGA) was considered for the electron-electron exchange and correlation interactions, in accordance to the Perdew-Wang 91 [20] parameterizations. Pseudopotentials of Al, In and N were constructed by taking into account $3s^2 3p^1$, $5s^2 5p^1$ and $2s^2 2p^3$ orbitals as respective valence electrons. For total and projected electron densities of states calculations, we opted for tetrahedron method and sampling of Brillouin zone was changed to Gamma centered grid with finer k-meshes of $11 \times 11 \times 11$.

While GGA exchange correlation functional is reliable when being used in calculations of ground state energy, it tends to underrate energy band gap values, due to derivative discontinuities and failure to precisely handle self-interaction of electrons in Hartree energy. These shortcomings prompted the need to widen the energy gaps via one-shot GW or G_0W_0 approximation [21]. Correction of band gap was implemented by means of ABINIT code [22] fixed with a k-point sampling of $4 \times 4 \times 4$ Monkhorst-Pack grids, 35 Hartree cut-off energy and 150 bands, as suggested by prior convergence studies. To begin, ground state estimation on optimized structure was performed till converged. This was followed by the computations of eigenvalues and eigenfunctions for Kohn Sham formulism at ground electronic state. Next, calculations of the screened interaction W_0 and self-energy matrix came into frame. Screening part was treated using Plasmon-pole model of Hybertsen and Louie [23], whereby the pole parameters were acquired through dielectric matrix computed only at zero frequency. We set kssform = 3, in which the Kohn Sham structure was generated through conjugate gradient algorithm. This setting allowed values of nband and nbandkss to be matched. In our case, scissor shift refers to the band gap distinction between GGA and GWA computations.

3. Results and discussion

3.1. Crystal structure determination

Stable structures within Al–In–N system can be identified through convex hull drawing, which links the stable phases against alteration and decomposition into other possible ternary forms. Alloy with the most negative formation enthalpy per block is chosen to be the thermodynamically stable one. The formation enthalpy of $Al_xIn_{1-x}N$ is evaluated using the equation

$$\Delta H(Al_xIn_{1-x}N) = H(Al_xIn_{1-x}N) - xH(AlN) - (1-x)H(InN)$$

where x denotes the concentration of AlN. As shown in Fig. 1, the evolutionary screening unlocked a global minimum structure, the orthorhombic $Cmc2_1$-$Al_4In_2N_6$. Its Al, In, N1 and N2 atoms occupy the Wyckoff 8b (0.32852, 0.33649, −0.43980), 4a (0.00000, 0.32230, −0.44455), 4a (0.00000, −0.29973, 0.47446) and 8b (−0.18443, 0.14903, 0.42509) sites, respectively. In addition, five practically stable compounds were identified, namely the trigonal crystals $AlIn_7N_8$ ($P3m1$) and Al_5InN_6 ($P31m$) plus monoclinic structures $Al_2In_4N_6$ (Cc/Aa), $Al_3In_3N_6$ (Cm/Am) and $Al_6In_2N_8$ ($P2_1$). The optimized unit cells of the six stable phases are shown in Fig. 2. Each of these compositions was verified using fixed composition mode, with its prior optimized structure being added as seed.

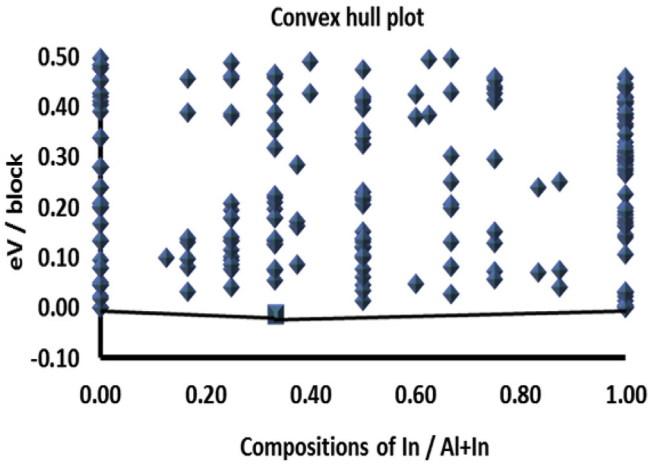

Fig. 1. Convex hull plot for Al–In–N system identified by USPEX. Filled square signifies global minimum structure.

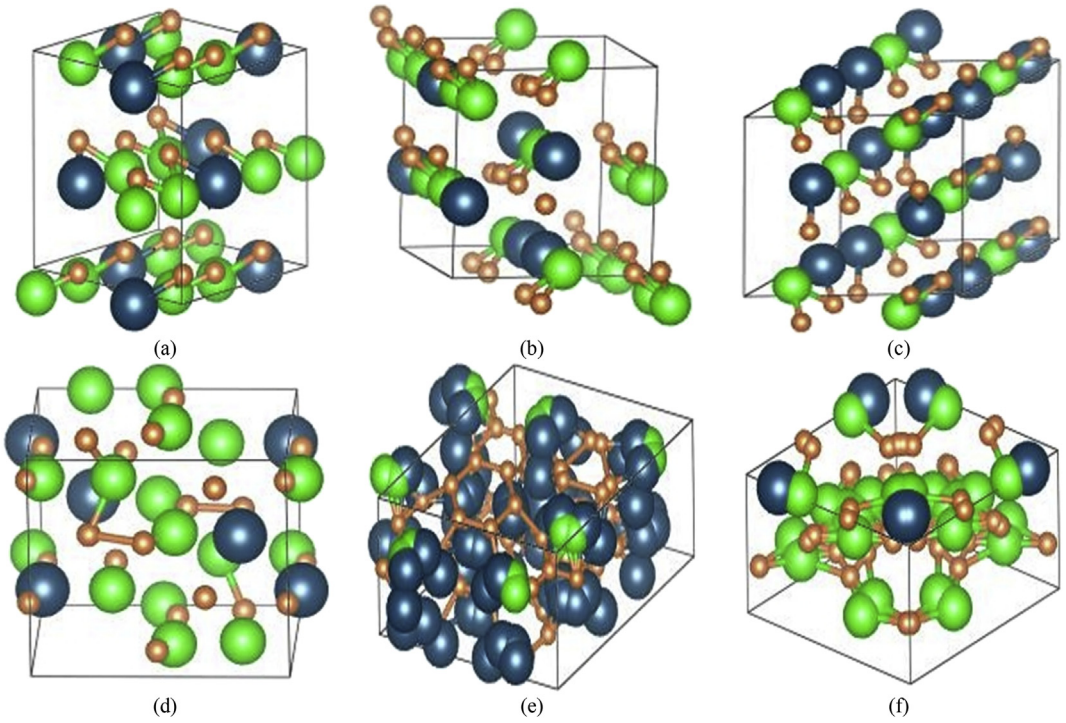

Fig. 2. Unit cells and structures of (a) $Al_4In_2N_6$ ($Cmc2_1$), (b) $Al_3In_3N_6$ (Cm/Am), (c) $Al_2In_4N_6$ (Cc/Aa), (d) $Al_6In_2N_8$ ($P2_1$), (e) $AlIn_7N_8$ ($P3m1$) and (f) Al_5InN_6 ($P31m$) at atmospheric pressure. Large blue, medium green and small amber spheres represent indium, aluminium and nitride ions.

Output such as formation enthalpy, symmetry and lattice parameters for abovementioned phases are consistent with findings obtained from variable composition runs. The crystallographic data and formation enthalpies of stable $Al_xIn_{1-x}N$ crystals are displayed in Table 1. At one of the extremes, stable phase for InN is rightly predicted to be hexagonal $P6_3mc$. When comparing the predicted lattice constants of wurtzite InN with experimental result [24], we find that the differences in percentage are 0.85% and 1.18% for *a* and *c* lattice parameters, respectively. As for AlN, the computed Cc/Aa stable structure is having energy per atom that is somehow lower than the empirically proven wurtzite $P6_3mc$. The energy difference is rather minimal, less than 1.0 meV/atom and is likely due to the fact that GGA functional does at times marginally overestimate crystal structure stability [25]. It is also worth noting that as the concentration of Al or In declines from extreme points to proportion of universal minimum (Table 2), the AlN–InN alloy undergoes a trigonal to monoclinic transition, and then transforms to an orthorhombic phase.

To further determine the composition dependence of lattice constant in $Al_xIn_{1-x}N$ alloy, curve fitting in Fig. 3 was employed. Notably, *a* lattice constant is decreasing monotonically with an increase in aluminium composition. In contrast, dependence of *c* lattice constant on aluminium composition is quite irregular. Deviation parameter, given by coefficient of x^2, is 4.233 Å for *a* lattice constant and −3.537 Å for *c* lattice constant. Large lattice bowing in *a* and *c* demonstrate that the size effects associated with difference in ionic radius between Al and In are strong.

Table 1
Lattice constants and enthalpies per block for stable compounds in Al–In–N system.

Compound	eV/block	Lattice constant (Å)	
$Al_4In_2N_6$	−0.0114	a = 5.568	
		b = 5.551	
		c = 5.146	
$Al_3In_3N_6$	0.0135	a = 5.680	
		b = 5.268	
		c = 5.680	
$Al_2In_4N_6$	0.0278	a = 5.808	
		b = 5.808	
		c = 6.300	
$Al_6In_2N_8$	0.0411	a = 5.504	
		b = 5.088	
		c = 6.381	
$Al_1In_7N_8$	0.0414	a = 6.889	
		c = 5.539	
$Al_5In_1N_6$	0.0306	a = 5.450	
		c = 5.054	
Wurtzite InN	0.0000	a = 3.503	[24]
		c = 5.626	
		a = 3.533	
		c = 5.693	

3.2. Electronic structure computations

Density of states and electronic band structure provide useful information needed for a detailed breakdown of physical properties of a substance. The energy band structure, total and site projected densities of states for all stable compounds listed in Table 1 are presented in Figs. 5 and 6. As highlighted in Fig. 5, GGA approach

Table 2
Space group (SG), GGA band gap and scissor shift for different phases.

Phase	SG	GGA gap/eV	Scissor shift/eV
$Al_5In_1N_6$	157	3.291	2.202
$Al_6In_2N_8$	4	2.794	1.793
$Al_4In_2N_6$	36	2.555	1.778
$Al_3In_3N_6$	8	1.758	1.219
$Al_2In_4N_6$	9	1.088	0.718
$Al_1In_7N_8$	156	0.331	0.155

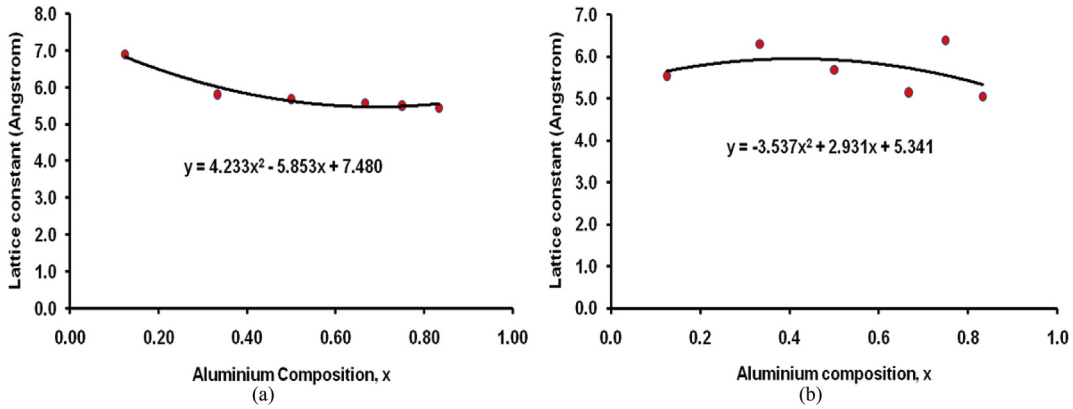

Fig. 3. The (a) *a* and (b) *c* lattice constants of $Al_xIn_{1-x}N$ alloy as a function of aluminium composition.

indicates that all the chosen stable compounds fit into the direct band gap semiconductor group, in which minimum of conduction band and maximum of valence band share identical k-vector. It is also noted that curvature of dispersion curve at conduction band minimum in all cases appears larger than one at valence band maximum. Hence, higher mobility and smaller effective mass (m*) for electron than for holes are projected. $AlIn_7N_8$ ($P3m1$) is likely to have smallest m* for both electrons and holes due to curvier bands at extrema, as a result of level repulsion.

What is more, the GW approximation succeeded in broadening the energy band gap of all desired structures by around 40%. Subsequently, the nonlinear interpolation equation of composition dependence energy band gap E_g for composites in $Al_xIn_{1-x}N$ was plotted and is given by:

$$E_g(x) = 1.235x^2 + 4.806x + 0.298$$

The fitting of E_g in Fig. 4 displays a value of R^2 (coefficient of determination) greater than 95%, epitomizing a reliable predictor of E_g on the dependent variable x. As Al composition increases, band gap is widened.

Note that the bowing parameter of 1.235 eV is remarkably small when compared to previously published work of others [26,27], implying slight deviation from linear behavior. In PDOS analysis, GGA results display a separation of valence band into two sub-bands (see Fig. 6). Main occupants in the lower energies sub-band are N 2s states whereas the higher one is dominated by N 2p states, which also serve as primary electron conduction.

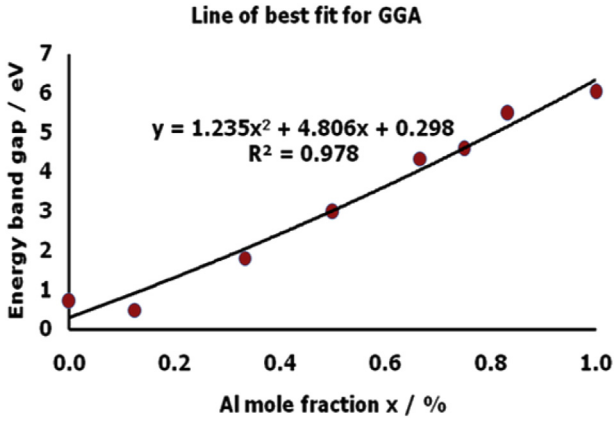

Fig. 4. Corrected energy band gap of $Al_xIn_{1-x}N$ system versus percentage of Al mole fraction in range of $0 \leq x \leq 1$.

Comparatively, N 2s orbitals are more tightly bound due to its farther downward position in the valence band. Hybridization is less prevalent in lower valence band, therefore contributing little or immaterially to bonding.

On the contrary, occurrence of stronger hybridization is noticed in upper valence band of all designated stable alloys. Inputs from p orbitals pairing of N–I and N–Al are diffused with close resembling weighs. Between −6.0 and 0.0 eV, imbrications of N 2p and In 5p orbitals are seen in $Al_2In_4N_6$ and $AlIn_7N_8$ while remaining structures, except $Al_3In_3N_6$, are of overlaps between N 2p and Al 3p states, with some contributions from Al 3s. For $Al_3In_3N_6$, strong hybridization is seen between N 2p, Al 3p and In 5p, resulting in a thick band across −4.0 to −1.5 eV, as shown in Fig. 5(b). Pi bonds from these overlaps indicate the subsistence of mild covalency in all stable compounds. There is no presence of deep valley or pseudo-gap feature around Fermi level in DOS plots. However, there are valleys around −4.0 eV mark for the six alloys. These traits point to the incidence of weakened bonding states between N 2p and Al 3s (In 5s) orbitals when moving beyond −4.0 eV. Shape of total DOS and peak location for selected $Al_xIn1_{-x}N$ structures also appear fairly dissimilar, which suggests a strong reliance of band structure on the contents of Al and In. To gain better understanding of the bonding character, electron density analysis was carried out using Atoms in Molecules theory developed by Bader [28,29]. Table 3 shows the average charge transported per atom for Al, In and N in each stable compound. Considerable amounts of charge transfer between cation-anion pairs are observed. Together with hybridization patterns that appear in upper valence band of all stable structures, the Bader analysis confirm the existence of mixed bonding nature in the six compounds. The mixed bonding in them is of ionic-covalent type.

4. Conclusions

In summary, widespread investigations of stable alloys within AlN–InN scheme have been performed at atmospheric pressure using hybrid evolutionary algorithm in variable compositions mode. Calculations were sampled at 4–8, 8–16 and 10–20 atoms size. Besides identifying orthorhombic $Al_4In_2N_6$ ($Cmc2_1$) as the thermodynamically stable one, the explorations also uncovered five more ternary structures, specifically $AlIn_7N_8$ ($P3m1$), Al_5InN_6 ($P31m$), $Al_2In_4N_6$ (Cc/Aa), $Al_3In_3N_6$ (Cm/Am) and $Al_6In_2N_8$ ($P2_1$). All these structures have mixed bonding with fractions of ionic and covalent components as exhibited by their hybrid characters and Bader analysis results. Corrected band gap values in these structures are directly proportional to amount of aluminium constituent.

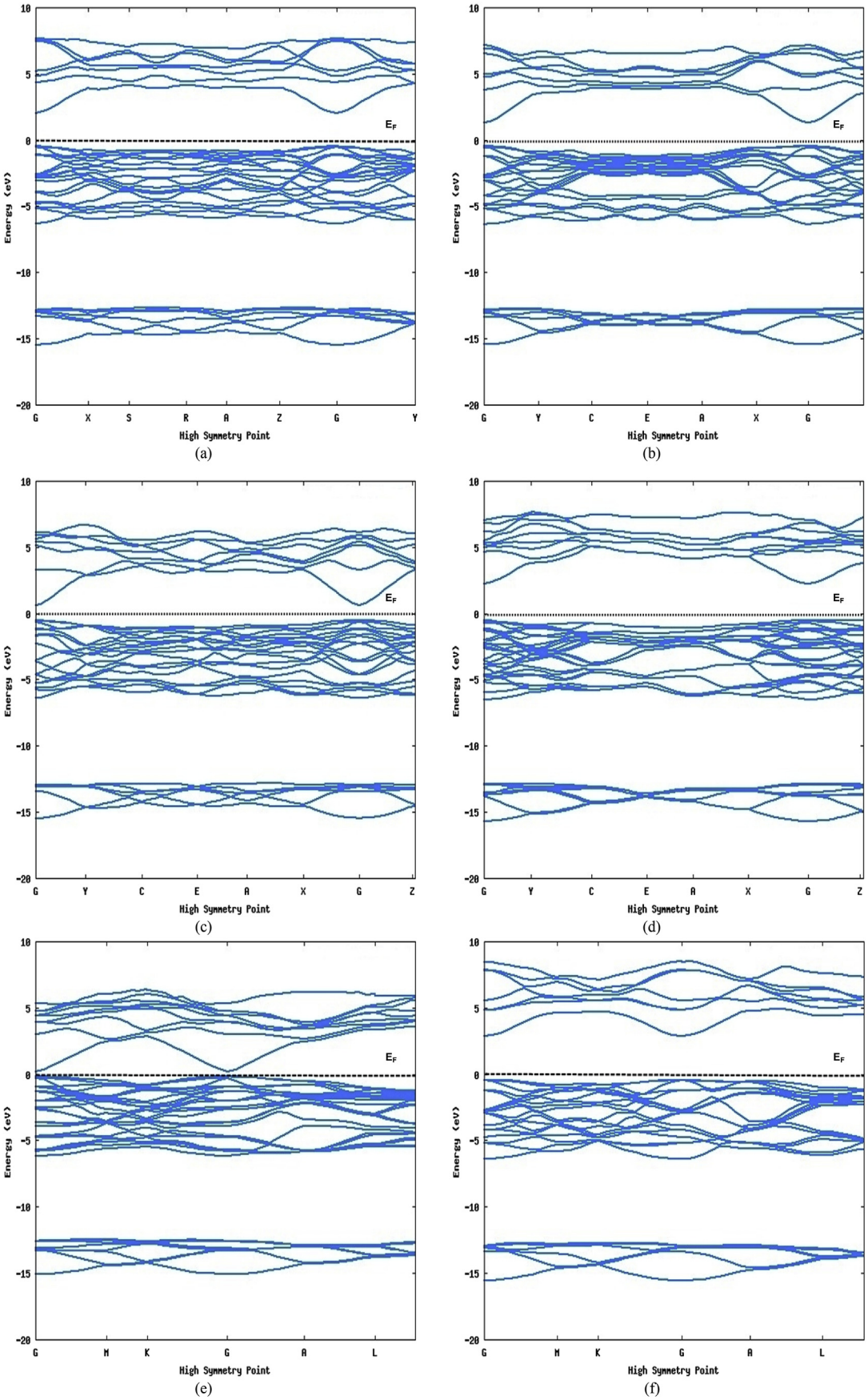

Fig. 5. Electronic band structure within GGA for (a) $Al_4In_2N_6$ (b) $Al_3In_3N_6$ (c) $Al_2In_4N_6$ (d) $Al_6In_2N_8$ (e) $AlIn_7N_8$ (f) Al_5InN_6 compounds. Horizontal dotted lines denote Fermi level.

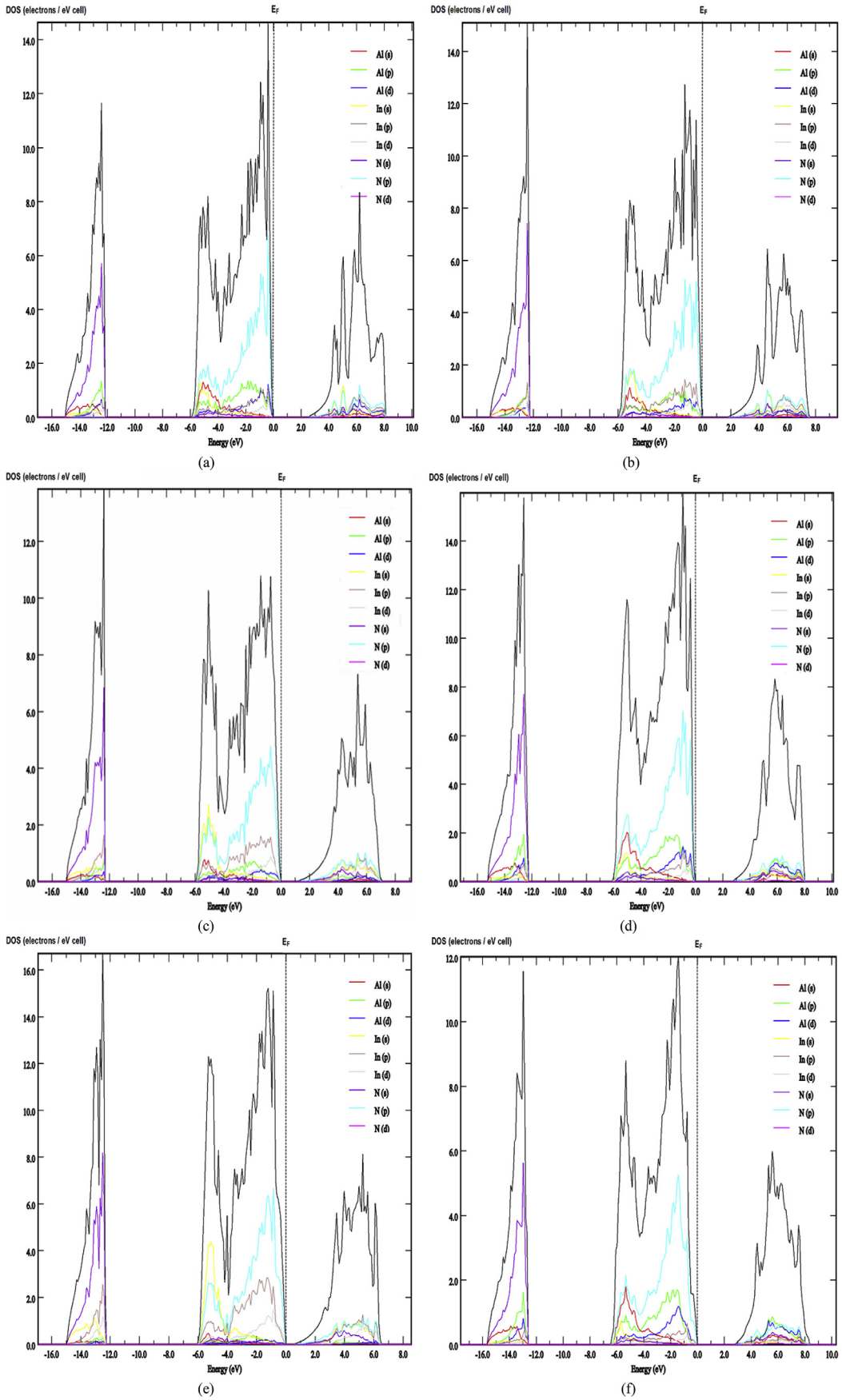

Fig. 6. Total and projected densities of states within GGA for (a) $Al_4In_2N_6$ (b) $Al_3In_3N_6$ (c) $Al_2In_4N_6$ (d) $Al_6In_2N_8$ (e) $AlIn_7N_8$ (f) Al_5InN_6 compounds. Vertical dotted lines represent Fermi energy.

Table 3
Charge transfer activities among Al, In and N ions. Main donors are marked in bold.

Compound	Atom type	Mean charge transferred/received* per atom
$Al_4In_2N_6$	**Al**	2.135
	In	1.501
	N	1.924*
$Al_3In_3N_6$	**Al**	2.037
	In	1.677
	N	1.857*
$Al_2In_4N_6$	Al	1.920
	In	1.447
	N	1.605*
$Al_6In_2N_8$	**Al**	2.038
	In	1.426
	N	1.885*
$Al_1In_7N_8$	Al	1.670
	In	1.302
	N	1.348*
$Al_5In_1N_6$	**Al**	1.806
	In	1.091
	N	1.686*

Acknowledgments

Authors would like to acknowledge the support of FRGS Grant (FASA 2/2013) by the Ministry of Higher Education of Malaysia (203/PFIZIK/6711348). Immense recognition must also be rendered to all Theory and Computational Laboratory personnel for their support and constructive inputs.

References

[1] Y.F. Wu, A. Saxler, M. Moore, R.P. Smith, S. Sheppard, P.M. Chavarkar, T. Wisleder, U.K. Mishra, P. Parikh, IEEE Electron Device Lett. 25 (2004) 117.
[2] L.I. Berger, Semiconductor Materials, CRCPress, 1997. ISBN: 0-8493-8912-7 123–124.
[3] C.G. Ma, V. Krasnenko, M.G. Brik, An ab initio study of the "direct–indirect bandgap" transition in $Al_xIn_{1-x}P$ alloys, Solid State Commun. 205 (2015) 55–60.
[4] T. Onuma, S.F. Chichibu, Y. Uchinuma, T. Sota, S. Yamaguchi, S. Kamiyama, H. Amano, I. Akasaki, J. Appl. Phys. 94 (2003) 2449.
[5] A.T. Cheng, Y.K. Su, W.C. Lai, Y.Z. Chen, S.Y. Kuo, J. Electron. Mater. 37 (2008) 1070.
[6] K. Lorenz, N. Franco, E. Alves, I.M. Watson, R.W. Martin, K.P. O'Donnell, Phys. Rev. Lett. 97 (2006) 085501.
[7] R. Butte, et al., Current status of AlInN layers lattice-matched to GaN for photonics and electronics, J. Phys. D. Appl. Phys. 40 (2007) 6328–6344.
[8] M.M. Satter, et al., Design and analysis of 250-nm AlInN laser diodes on AlN substrates using tapered electron blocking layers, IEEE J. Quantum Electron. 48 (2012) 703–711.
[9] C.K. Tan, N. Tansu, Gain and spontaneous emission characteristics of AlInN quantum well for deep ultraviolet emitters, Proc. IEEE Photonics Conf. 577–578 (2015).
[10] B.T. Liou, S.H. Yen, Y.K. Kuo, Vegard's law deviation in band gap and bowing parameter of $Al_xIn_{1-x}N$, Appl. Phys. A 81 (2005) 651–655.
[11] Bo-Ting Liou, Chieh-Wen Liu, Electronic and structural properties of zinc-blende $Al_xIn_{1-x}N$, Opt. Commun. 274 (2007) 361–365.
[12] Fei Wang, S.F. Li, Qiang Sun, Yu Jia, First principles study of structural and electronic properties of zincblende $Al_xIn_{1-x}N$, Solid State Sci. 12 (2010) 1641–1644.
[13] A.R. Oganov, C.W. Glass, Crystal structure prediction using evolutionary algorithms: principles and applications, J. Chem. Phys. 124 (24) (2006) 244704.
[14] A.R. Oganov, H. Stokes, M. Valle, How evolutionary crystal structure prediction works - and why, Acc. Chem. Res. 44 (3) (2011) 227–237.
[15] A.O. Lyakhov, A.R. Oganov, H. Stokes, Q. Zhu, New developments in evolutionary structure prediction algorithm USPEX, Comp. Phys. Comm. (2013) 1172–1182.
[16] G. Kresse, J. Furthmüller, Efficient iterative schemes for ab initio total-energy calculations using a plane-wave basis set, Phys. Rev. B 54 (1996) 11169.
[17] G. Kresse, J. Furthmüller, Efficiency of ab-initio total energy calculations for metals and semiconductors using a plane-wave basis set, Comput. Mat. Sci. 6 (1996) 15.
[18] A.O. Lyakhov, A.R. Oganov, M. Valle, Crystal structure prediction using evolutionary approach, Condens. Matter., in: A.R. Oganov (Ed.), Modern Methods of Crystal Structure Prediction, Wiley-VCH, Berlin, 2010.
[19] A.R. Oganov, Y. Ma, A.O. Lyakhov, M. Valle, C. Gatti, Evolutionary crystal structure prediction as a method for the discovery of minerals and materials, Rev. Mineral. Geochem. 71 (1) (2010) 271–298.
[20] J. Perdew, Y. Wang, Phys. Rev. B 45 (1992) 13244.
[21] F. Aryasetiawany, O. Gunnarsson, The GW method, Rep. Prog. Phys. 61 (1998) 237–312.
[22] X. Gonze, G.-M. Rignanese, M. Verstraete, J.-M. Beuken, Y. Pouillon, R. Caracas, F. Jollet, M. Torrent, G. Zerah, M. Mikami, Ph. Ghosez, M. Veithen, J.-Y. Raty, V. Olevano, F. Bruneval, L. Reining, R. Godby, G. Onida, D.R. Hamann, D.C. Allan, A brief introduction to the ABINIT software package, Z. Krist. 220 (2005) 558–562.
[23] M.S. Hybertsen, S.G. Louie, Phys. Rev. B 34 (1986) 5390.
[24] A. Zubrilov, in: M.E. Levinshtein, S.L. Rumyantsev, M.S. Shur (Eds.), Properties of Advanced Semiconductor Materials GaN, AlN, InN, BN, SiC, SiGe, John Wiley & Sons, Inc., New York, 2001, pp. 49–66.
[25] D. Aberg, B. Sadigh, J. Crowhurst, A.F. Goncharov, Thermodynamic ground states of platinum metal nitrides, Phys. Rev. Lett. 100 (2008) 095501.
[26] M. Van Schilfgaarde, A. Sher, A.-B. Chen, J. Cryst. Growth 178 (1997) 8.
[27] M. Goano, E. Bellotti, E. Ghillino, C. Garetto, G. Ghione, K.F. Brennan, J. Appl. Phys. 88 (2000) 6476.
[28] W. Tang, E. Sanville, G. Henkelman, A grid-based Bader analysis algorithm without lattice bias, J. Phys. Condens. Matter 21 (2009) 084204.
[29] E. Sanville, S.D. Kenny, R. Smith, G. Henkelman An, Improved grid-based algorithm for Bader charge allocation, J. Comp. Chem. 28 (2007) 899–908.